9 SCIENTIFIC HIGHLIGHT OF THE MONTH

Partial dislocations in wurtzite GaN

J. Kioseoglou, G. P. Dimitrakopulos, Ph. Komninou, H. M. Polatoglou, and Th. Karakostas

Department of Physics, Aristotle University of Thessaloniki, GR-54124 Thessaloniki, Greece

Abstract

The atomic structures and energies of $1/6 < 20\bar{2}3 >$ and $1/3 < 10\bar{1}0 >$ partial dislocations in wurtzite GaN are modelled using an empirical interatomic potential in combination with topological theory and anisotropic elasticity calculations. Twelve stable configurations of the $1/6 < 20\bar{2}3 >$ edge and mixed partial dislocations that bound I_1 intrinsic basal stacking faults are obtained for each polarity and their core radii, energies, and atomic configurations are given. Moreover, the $1/3 < 10\bar{1}0 >$ edge and mixed partial dislocations along the junction lines between inversion domain boundaries (IDBs) and I_1 stacking faults are studied. Twenty eight stable junction line configurations have been identified, sixteen of them resulting in stable transformations of the energetically favourable IDB* defect to the electrically active Holt type IDB. The majority of the dislocation core structures possessed either dangling bonds or highly strained bonds. Since reduced coordination or strained bonds can introduce gap states, such dislocations could be electrically active.

1. Introduction

The influence of dislocations on the electrical, optical and mechanical properties of Ga-based III-nitride semiconductors is currently under intense investigation. Efficient optical devices such as blue-light-emitting diodes are commercially available despite the presence of a high density ($\sim 10^9$ cm^{-2}) of threading dislocations [1]. Theoretical and experimental investigations so far have concentrated on lattice dislocations. Initial theoretical results using *ab initio* calculations

indicated that charge-neutral edge and screw threading dislocations do not contribute to gap states and they are electrical inactive [2]. This has been disputed by other *ab initio* studies which have shown that edge dislocations may be charged, giving rise to deep-gap states [3], [4]. Dependence of the core formation energies on the Fermi level and growth stoichiometry has also been examined [3]. Moreover tight binding calculations have shown evidence for empty gap states associated with edge dislocations in the top half of the gap [5]. Also, by the use of first-principles calculations of electron energy-loss spectra, has been shown gap stage associated with edge dislocations [6]. Regarding the screw dislocations, full core structure has been observed using Z-contrast imaging [7] and the open core structure by transmission electron microscopy, [8] [9] while their electrical activity has been related to the growth stoichiometry [10]. More recently new structures for the screw dislocation have been proposed under certain growth conditions [11] [12].

Beside the perfect lattice dislocations, optoelectronic properties of devices should be also influenced by the partial dislocations when they exist in large numbers. The aim of the present contribution is to perform a systematic investigation of the core structures and the corresponding energies of the $1/6 < 20\bar{2}3 >$ edge and mixed partial dislocations that bound I_1 intrinsic basal stacking faults in wurtzite GaN, and of the $1/3 < 10\bar{1}0 >$ edge and mixed partial dislocations along the junction lines between inversion domain boundaries (IDBs) and I_1 stacking faults (SFs). Core radii and energies are evaluated in an approach combining anisotropic elasticity, topological theory and atomistic calculations. Initially, the dislocation displacement field of the $1/6 < 20\bar{2}3 >$ edge and mixed partial dislocations is imposed according to anisotropic elasticity theory [13]. For the IDB-I_1SF junction line, the initial configurations are based on Volterra models. In both cases the supecells are relaxed to the minimum energy by the use of an interatomic potential.

In order to achieve a satisfactory description of the microstructure and the energetics of junctions between extended defects, a large number of atoms must be taken into account. Although the energies of many of the isolated planar defects observed in epitaxial GaN layers have been determined using *ab initio* calculations, the total energy of large scale atomic configurations involving different planar defects cannot be calculated, for supercells exceed 15,000 atoms. For this purpose, an empirical potential of the Stillinger-Weber type [14], can be employed; this potential has previously been successfully applied for the study of line and extended defects in GaN [15] [16] [17] [18] [19] [20]. The use of an empirical potential in order to describe the structures and energetics of dislocations is certainly less accurate in comparison with a tight-binding approach or *ab initio* calculations, since it does not consider explicitly the electronic effects. Tight-binding or *ab initio* calculations employ mainly two approaches in order to model dislocations. In the first approach a dislocation dipole or multipole is placed in a supercell and this leads to a considerable interaction between dislocations. In the second approach, where an isolated dislocation is considered in a supercell-cluster with periodic boundary conditions along the dislocation line and hydrogen-terminated surfaces parallel to the line direction, the long range elastic effects are not treated rigorously [6] [21] [22]. On the other hand however, in dislocation modeling, medium and long range strain effects play an important role and the empirical potential offers better embedding of the core into the surrounding bulk material. The advantages of the empirical potential calculations are the competency to treat thousands of

atoms and the efficient way to take into account fixed boundary conditions in surfaces parallel to the line direction of the dislocation far from the core area. The strain induced by the dislocation in this case is more accurately estimated. Since the stress of the supercell geometry influences the core structure and the core energy [23], it provides a better embedding of the core. Moreover, such calculations have been proven [24] suitable for treating relatively complicated supercells comprising multiple planar defects.

The material of this highlight has been presented in detail in three regular articles of Physical Review B. The topological analysis of the IDB-SF interactions and the characterization of experimental observations using circuit mapping technique and electron microscopy image simulations has been analysed in ref [25]. The atomic structures and energies of $1/6 < 20\bar{2}3 >$ partial dislocations delineating the I_1 intrinsic basal stacking fault in wurtzite GaN are modelled using an empirical interatomic potential in combination with anisotropic elasticity calculations in ref [26]. Finally the predicted IDB-SF interactions [25] have been analyzed at atomic scale using large scale empirical potential calculations in ref [27].

Our study is divided in two parts. In the first part the $1/6 < 20\bar{2}3 >$ partial dislocations are analysed. In section 2.1 the computational method is given. In section 2.2 the dislocation parameters are calculated using elasticity theory and empirical potential calculations. In the second part and in section 3.1 the topological methodology is outlined and the admissible junctions between IDBs and basal I_1 SFs are determined. The relaxed atomic configurations and their energies are presented in section 3.2. Finally, in section 4 the main conclusions of our study are presented.

2. I_1 SF Partial Dislocations

2.1 Computational Method

The GaN structure (spacegroup$P6_3mc$) [28] consists of four atoms per unit cell and can be visualized as two interpenetrating hexagonal substructures, one of Ga and one of N atoms related by a spacing u along the c-axis. The position vectors of the atoms comprising the crystal's motif are $\mathbf{u}_A$=1/12 [40$\bar{4}$3], $\mathbf{u}_B$=1/12 [$\bar{4}$04$\bar{3}$] for atoms of the one species, and $\mathbf{u}_a$=1/12 [40$\bar{4}$3] + u [0001], $\mathbf{u}_b$=1/12 [$\bar{4}$04$\bar{3}$] + u [0001] for atoms of the other species [29]. For the GaN wurtzite structure, c/a= 1.626, u= 0.375 and the coordination number is 4 [1].

The stacking sequence for the perfect wurtzite structure along [0001] is ... $AaBbAaBbAaBb$ ..., i.e. each layer parallel to the basal plane is composed of two sublayers of distinct atomic species (aB or bA where capital and small fonts denotes distinct atomic species.) (figure 1(a)).

In the wurtzite structure, two types of intrinsic SFs, designated I_1 and I_2, and one extrinsic, designated E, can be formed [13]. These are low-energy defects since they do not disturb the nearest-neighbor packing. The I_1 intrinsic SF (figure 1(b)) corresponds to one violation of the stacking rule and can be formed by the removal of a B plane followed by shearing by $1/3 < 10\bar{1}0 >$ (figure 2).

In order to describe the I_1 SF configuration with bounding partial dislocations, we start from the perfect crystal [13]. Upon removal or addition of a basal disc of atoms (vacancy or interstitial

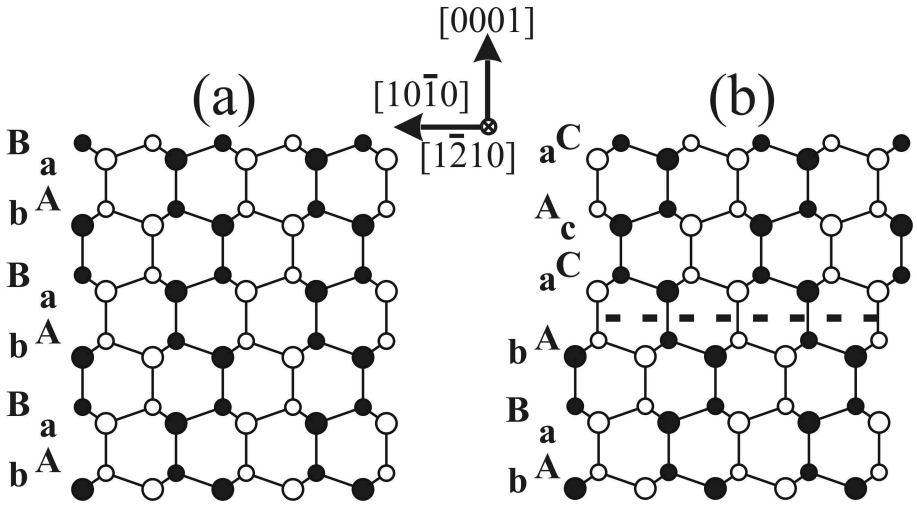

Figure 1: (a) Wurtzite structure and (b) I_1 SF projected along the $< 1\bar{2}10 >$ direction. The broken line indicates the SF plane, large and small circles denote distinct atomic species, unfilled circles are at 0 level, and filled circles are at level $a/2$ along the projection direction.

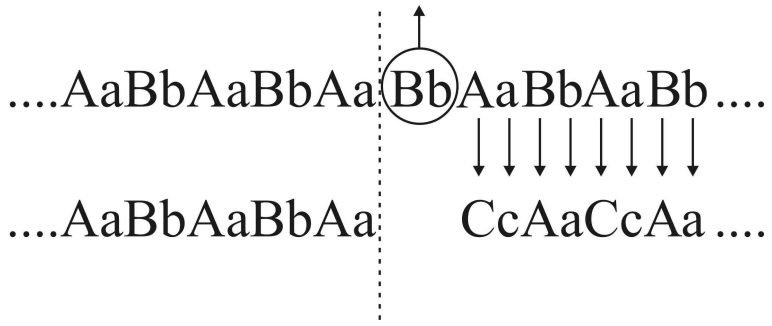

Figure 2: The stacking sequence in the formation of a I_1 SF.

disc) and assuming that only displacements normal to the basal plane are associated with the precipitation, the SF is bounded by a Frank loop with Burgers vectors 1/2[0001] [13]. A loop of Shockley partial dislocation is then nucleated in the faulted region leading to the formation of I_1 SF. In other words, if a shear is associated with vacancy (case a) or interstitial disc precipitation (case b) the I_1 type fault could be formed. The above SFs are bounded by loops comprising edge and mixed segments with Burgers vectors:

$$b_e = 1/2[0001] + 1/3[10\bar{1}0] = 1/6[20\bar{2}3]$$

and

$$b_m = 1/2[0001] + 1/3[1\bar{1}00] = 1/6[2\bar{2}03]$$

respectively (assuming a $[1\bar{2}10]$ segment line direction).

The supercells, for the $1/6 < 20\bar{2}3 >$ edge and mixed partial dislocations, initially contained perfect crystal of wurtzite GaN. By employing displacements expected from anisotropic elacticity theory [13], the unrelaxed structures of the I_1 intrinsic SF and the corresponding partial dislocation were formed to be used as initial atomic positions. The supercells were created in the form of rectangular parallelepiped volumes. Periodic boundary conditions were applied along the dislocation line direction (i.e. $[1\bar{2}10]$), while fixed boundaries were imposed perpendicular to the dislocation line, thus following the so-called "hybrid" model [22]. The fixed boundary conditions were applied using the following methodology (figure 3): perpendicular to the dislocation line the supercell was divided into three concentric domains defining a thin external domain, a thin intermediate domain and the internal area with the dislocation line at the centre. The thickness of the external domain is larger than the maximum range of the potential (3.36 Å for the Ga-Ga interaction [19]), and the atoms are at fixed positions there. The intermediate domain starts at the end of the external one and also extends further than the maximum range of the potential and up to the internal area. In the intermediate domain the atoms are relaxed but are not taken into account in energetic calculations. The energetic calculations are evaluated taking into consideration only the energies of the relaxed atoms in the internal area. (Although test calculations have shown that in most cases the atoms in the intermediate domain are relaxed sufficiently well and their energies could also have been taken into account. It has been found that the deviation of the atomic energies in the intermediate domain, due to their vicinity with fixed atoms, is inversely proportional to the size of the supercell and for the supercells used in the present cases it is very small. Nevertheless the intermediate domain has been excluded from our calculations.)

For the relaxation, the modified [19] [20] Stillinger-Weber potential (MSWp) has been employed.

The Stillinger-Weber [14] potential (SWp) attempts to model a semiconductor in a semiclassical way and it is based on a two-body term:

$$\begin{cases} v_2(r_{ij}) = \varepsilon A(B(\frac{r_{ij}}{\sigma})^{-4} - 1)exp[((\frac{r_{ij}}{\sigma}) - \alpha)^{-1}] for \frac{r_{ij}}{\sigma} < \alpha \\ v_2(r_{ij}) = 0 for \frac{r_{ij}}{\sigma} \geq \alpha \end{cases} \quad (1)$$

and a three body term:

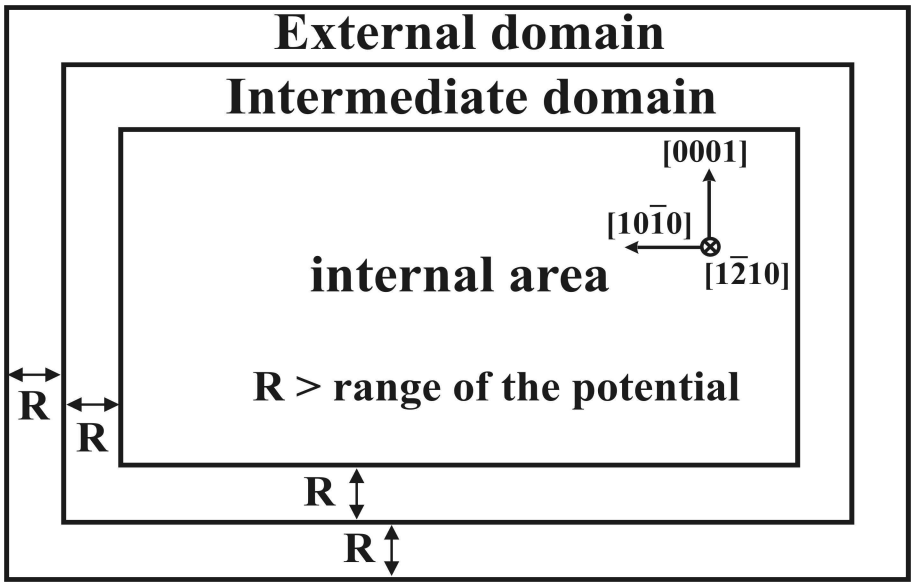

Figure 3: Schematic illustration of the fixed boundary methodology.

$$v_3(r_{ij},r_{ik},\theta_{ijk}) = \varepsilon\ \lambda\ \exp[\gamma\ (r_{ij}\ -\ \alpha\ )^{\ -\ 1} + \gamma\ (r_{ik}\ -\ \alpha\ )^{\ -\ 1}]\ x\ (\cos\ \theta_{\ ijk} + \theta_{\ 0})^2 \qquad (2)$$

where ε and σ are the energy and length units; A, B, α are positive, α represents the cut-off distance, and θ_{ijk} is the angle subtended by the ji and the jk bond. The original SWp takes into account 7 parameters (α, γ, σ, ε, A, B, λ). However, its build-in tetrahedral bias of one kind of bonds creates problems in other situations; it is necessary to take into account 21 parameters in order to represent the three kinds of bonds in GaN (*i.e.* Ga-N, and Ga-Ga or N-N "wrong" bonds). In table 1 we present the SWp parameters.

Type of bond	α	γ	σ **(a.u.)**	ε **(eV)**	**A**	**B**	λ	θ_0
Ga-N	1.8	1.2	3.203	2.17	7.917	0.720	32.50	1/3
Ga-Ga	1.6	1.2	3.968	1.2	7.917	0.720	26.76	1/3
N-N	1.8	1.2	2.457	1.2	7.917	0.720	26.76	1/3

Table 1: Parameters of the modified Stillinger-Weber potential. (α, γ, A, B, λ and θ_0 dimensionless)

The minimum energy configurations were obtained using the quench molecular dynamics method [30]. We assumed bonds between atoms within distances up to 2.4 Å in all atomic configurations which is the minimum range of the MSWp (for the N-N interaction [19]).

Generally, atomistic empirical potential calculations provide the total energy of a relaxed structure. Let E^{excess}_{TOTAL} be the total excess energy of a supercell, defined as the difference between the total energy found by empirical potential calculations and the energy of a supercell of perfect

GaN crystal containing the same number of atoms. Let also $\mathrm{E}_{\mathrm{planar\,defect}}$ be the planar defect energy per unit area, i.e. the total excess energy of a supercell containing the planar defect divided by planar defect area. $\mathrm{E}_{\mathrm{planar\,defect}}$ was evaluated by relaxing a supercell containing a planar defect in the middle; periodic boundary condition were employed along all three directions.

The I_1 SF has been found to have formation energy equal to 1.8 meV/Å^2 which is in satisfactory agreement with the value of 1.1 meV/Å^2 given by *ab initio* [31].

The dislocation energy per unit length, $E_d(R)$, of each dislocation in a cylinder of radius R was calculated as the total excess energy of the cylinder minus the sum of the planar defects energies.

Hence

$$E_d(R) = \frac{E^{excess}_{TOTAL}(R) - \sum\limits_{planar\,defects} E_{planar\,defect} \times (planar\,defect_{area}(R))}{L} \tag{3}$$

where L is the length of the supercell along $[1\bar{2}10]$.

Continuum elasticity theory is complementary to atomistic simulations for the modeling of line defects since it allows an evaluation of the long range strain effects whereas atomistic simulations describe core structure and energy. The strain energy of an infinite straight dislocation in a perfect crystal can be calculated analytically using linear elasticity [13]. The total energy of a dislocation is equal to the elastic energy plus the core energy:

$$\mathrm{E}_{\mathrm{total}} = \mathrm{E}_{\mathrm{elastic}} + \mathrm{E}_{\mathrm{core}} \tag{4}$$

The elastic energy per unit length of a dislocation contained in a cylinder of radius R is given by

$$E_{elastic} = A \ln \frac{R}{r_0}, \quad r_0 \leq R \tag{5}$$

where $\mathrm{A} = \frac{\mathrm{Kb}^2}{4\pi}$ is the prelogarithmic factor, **b** is the Burgers vector, K is an energy factor and r_0 is the core radius.

Let xz be the basal plane where x is $[10\bar{1}0]$, and let the dislocation line $[1\bar{2}10]$ coincide with the z axis. The y axis, in this coordinate system is along the [0001] direction. The elastic energy of a dislocation in the basal plane can be decomposed into screw and edge parts according to anisotropic elasticity as follows [13]

$$E_{elastic} = \frac{1}{4\pi}(K_s b_s^2 + K_{e_x} b_{e_x}^2 + K_{e_y} b_{e_y}^2) ln \frac{R}{r_0} \tag{6}$$

where K_s is the energy factor of b_s, the screw component of the Burgers vector of the dislocation, and $\mathrm{K}_{\mathrm{e_X}}$, $\mathrm{K}_{\mathrm{e_Y}}$ are the energy factors of the edge components, $\mathrm{b}_{\mathrm{e_X}}$ and $\mathrm{b}_{\mathrm{e_Y}}$ respectively.

The energy factors are equal to [13]

$$K_s = (C_{44} C_{66})^{1/2}, \tag{7}$$

$$K_{e_x} = [(C_{11}C_{33})^{1/2} + C_{13}] * \{\frac{C_{44}[(C_{11}C_{33})^{1/2} - C_{13}]}{C_{33}[(C_{11}C_{33})^{1/2} + C_{13} + 2C_{44}]}\}^{1/2}, \quad (8)$$

And

$$K_{e_y} = [(C_{11}C_{33})^{1/2} + C_{13}] * \{\frac{C_{44}[(C_{11}C_{33})^{1/2} - C_{13}]}{C_{11}[(C_{11}C_{33})^{1/2} + C_{13} + 2C_{44}]}\}^{1/2} \quad (9)$$

where C_{11}, C_{13},C_{33}, C_{44} and C_{66} are the elastic constants.

As has been shown previously, two types of admissible partial dislocations may bound the I_1 SF. An edge dislocation with Burgers vector equal to $b_e = 1/6[20\bar{2}3]$ and a mixed-type dislocation with Burgers vector $b_m = 1/6[2\bar{2}03]$. In both cases the dislocation line is taken to be $[1\bar{2}10]$. Using the elasticity theory, the prelogarithmic factors for the edge and the mixed dislocations were calculated, as well as the ratio between them. The edge dislocation can be decomposed into two normal edge components $b_{\mathrm{e_X}} = 1/3\,[10\bar{1}0]$and $b_{\mathrm{e_Y}} = 1/2\,[0001]$ while the mixed dislocation can be decomposed into a screw $b_s = 1/6\,[1\bar{2}10]$ and two normal edge components $b_{\mathrm{e_X}} = 1/6\,[10\bar{1}0]$ and $b_{\mathrm{e_Y}} = 1/2\,[0001]$. Using elastic constants calculated by the MSWp [32], the prelogarithmic factors are found to be $A_e = 0.79\ eV/\mathring{A}$ and $A_m = 0.73\ eV/\mathring{A}$ leading to a ratio equal to $\frac{A_e}{A_m} = 1.08$. If experimental determined elastic constants [33] are used the prelogarithmic factors are $A_e = 0.82\ eV/\mathring{A}$ and $A_m = 0.76\ eV/\mathring{A}$, and the ratio between them again equals $\frac{A_e}{A_m} = 1.08$, i.e. due to the satisfactory agreement between the experimental and the calculated elastic constants [32], the obtained prelogarithmic factors are also in consistency.

The elastic energy of a dislocation is related to the radius of the cylinder and it is infinite for an infinite crystal. Although it can be calculated for a finite radius, it cannot be considered a characteristic invariable property like the core energy. Therefore, only the dislocation core energy, *i.e.* the energy of the minimum region which cannot be described by elasticity theory, can be used in such capacity.

In order to evaluate the core parameters of dislocations, the energy in the region bounded by coaxial cylinders of radii r and R_0 is plotted versusln(r), where R_0 is the external cylinder radius (taken as large as possible), and r is the internal cylinder radius ($r_0 \leq r \leq R_0$). The core radius r_0 is taken at the point where the curve stops being linear. Equation 5 can be written as:

$$\mathrm{E}_{elastic}(r) = A \ln R_0 - A \ln r \quad r \leq R_0. \quad (10)$$

The corresponding prelogarithmic factor is evaluated by fitting equation (10) to the calculated values. The core energy is evaluated by averaging the calculated energy values following equation (3) minus the elastic part:

$$\mathrm{E}_d(r) - \mathrm{E}_{elastic} = \mathrm{E}_d(r) - A \ln r + A \ln r_0. \quad r \geq r_0 \quad (11)$$

2.2 Results

In figure 4 the fully relaxed core structures of all the admissible atomic configurations are presented. Since, in [0001] orientation, the wurtzite structure presents two polarities (N or Ga

polarity), each atomic configuration is relaxed in both cases. In all atomic configurations we have assumed bonds between atoms within distances up to 2.4 Å which is the range of the MSWp for the N-N interaction (although the range for Ga-N and Ga-Ga interactions is larger than 3 Å) [19].

Following the procedure described in the previous section, figures 5 and 6 illustrate the energies $E_{elastic}(r)$ and $E_{core}(r) = E_d(r) - E_{elastic}$ versus $\ln(r)$ plots for partial dislocations delineating a I_1 SF formed by a collapsed vacancy disc or a precipitated interstitial loop respectively. In all cases, it can be observed that the curve becomes linear and the energy assumes the expression given by elasticity theory (eq. 10). In table 2 the calculated core radii, energies and prelogarithmic factors of the analyzed partial dislocations in both polarities of GaN are given. Also the prelogarihmic factors are presented as they have been evaluated by the use of elastic constants calculated with the MSWp ($A^{MSWp}_{elastic}$) and by the experimental elastic constants ($A^{\exp}_{elastic}$).

In the a-edge diagram of figure 5 we notice that the 5/7 core is energetically favorable for both polarities and it exhibits the smallest core radius. In the b-edge case, it is found that, as in a-edge case, the 5/7 core configuration has the lowest energy. These two core configurations are the lowest energy models between all the admissible dislocations and they are the only configurations in which all the atoms are tetrahedrally coordinated. The 8-atom rings (a-edge-b, a-edge-c and b-edge-b) and the 12-atom ring (b-edge-c) configurations include at least one atom with dangling bond and consequently require higher energies.

In the a-mixed diagram of figure 6 it is seen that the a-mixed-b configuration which exhibits a 5/7-atom ring has the smallest core and is energetically favorable. In the b-mixed diagram, it can be seen that the 12-atom ring of the b-mixed-a configuration is energetically favourable and presents the smallest core in comparison with the interstitial type b-mixed-b and c configurations.

Regarding the prelogarithmic factors, the calculated values given in table 2 are in agreement with the elasticity theory calculations. Discrepancies occur between the values for vacancy type b-edge-c configuration, and for, interstitial type, b-mixed-c configurations and the elastic theory calculated values. This divergence is related to the fitting process, in particular in determining the exact value where the curves become linear.

Partial dislocation	Core configuration	r_0 (Å)		E_{core} (eV/Å)		A (eV/Å)		$A^{MSWp}_{elastic}$ (eV/Å)	$A^{\exp}_{elastic}$ (eV/Å)
a-edge-a	5/7	2.0	(2.0)	0.50±0.02	(0.45±0.01)	0.79	(0.76)	0.79	0.82
a-edge-b	8	3.1	(3.1)	1.28±0.02	(1.34±0.02)	0.79	(0.79)	0.79	0.82
a-edge-c	8	3.1	(3.1)	1.34±0.02	(1.39±0.02)	0.78	(0.78)	0.79	0.82
b-edge-a	5/7	2.5	(2.5)	0.72±0.02	(0.76±0.02)	0.78	(0.76)	0.79	0.82
b-edge-b	8	2.5	(3.1)	1.34±0.02	(1.43±0.03)	0.75	(0.78)	0.79	0.82
b-edge-c	12	2.5	(2.5)	1.48±0.01	(1.39±0.01)	0.73	(0.73)	0.79	0.82
a-mixed-a	8	3.1	(3.1)	1.17±0.02	(1.17±0.02)	0.74	(0.74)	0.73	0.76
a-mixed-b	5/7	2.0	(2.0)	0.81±0.02	(0.96±0.02)	0.73	(0.72)	0.73	0.76

a-mixed-c	5/7	2.5	(3.1)	1.30±0.02	(1.48±0.02)	0.73	(0.75)	0.73	0.76
b-mixed-a	12	2.0	(2.0)	0.99±0.02	(1.05±0.02)	0.73	(0.72)	0.73	0.76
b-mixed-b	10	3.1	(3.1)	1.60±0.02	(1.83±0.03)	0.78	(0.83)	0.73	0.76
b-mixed-c	8	3.1	(3.1)	1.77±0.03	(1.66±0.04)	0.81	(0.87)	0.73	0.76

Table 2: The calculated core radii, energies and prelogarithmic factors of the $1/6 < 20\bar{2}3 >$ partial dislocations of GaN in N-polarity. The values for Ga-polarity are given in parentheses. The prelogarihmic factors obtained from anisotropic elasticity by the use of MSWp-calculated elastic constants ($A^{MSWp}_{elastic}$) and by the use of experimental elastic constants ($A^{\exp}_{elastic}$) are given.

In closing the discussion on $1/6 < 20\bar{2}3 >$ partial dislocations we remark that the obtained cores are structurally similar to those found favorable for perfect basal dislocations in GaN by *ab initio* calculations, [22] [34] as discussed in ref [26].

3. IDB-I_1 SF Junctions

3.1 Topological Analysis and Computational Method

A rigorous framework for the *a priori* characterisation of defects [29] [35] [36] has been applied in order to determine the defect character of IDB–SF junction lines [25]. This analysis is based on Volterra's description of line defects in elastic continua [37], as extended for bicrystals. For this purpose, the abutting crystal components, designated λ and μ, are initially considered to be joined along their interface with no long-range stresses present (figure 7(a)). A Volterra cut is then introduced along a part of their interface, and the exposed surfaces are modified by the addition/removal of material and/or the application of tractions as shown in figure 7(b). After re-joining the exposed surfaces, a line defect results between the initial interface and the new one. In agreement with the right-handed/finish-start (RH/FS) convention, this defect is described by the rigid-body operation required in order to bring the new μ surface onto the new λ one [29] [35] [36]. Let the new surfaces be obtained from the initial ones by the rigid-body operations $\mathcal{V}(\lambda)_{\rm j}$ and $\mathcal{V}(\mu)_{\rm i}$, where $\mathcal{V}(\lambda)_{\rm j} = (\mathbf{V}(\lambda)_j, \mathbf{v}(\lambda)_j)$ in Seitz notation [38] (with $\mathbf{V}(\lambda)_j$ being the orthogonal part and $\mathbf{v}(\lambda)_j$ the translation part of the operation), and similarly for $\mathcal{V}(\mu)_{\rangle}$.

Then the line defect is described by the operation [29] [35] [36]

$$\mathcal{Z}_{\rm ij} = \mathcal{V}(\lambda)_{\rm j}\, \mathcal{P}\, \mathcal{V}(\mu)_{\rm i}^{-1}\, \mathcal{P}^{-1}, \tag{12}$$

where $\mathcal{P} = (\mathbf{P}, \mathbf{p})$ is the transformation relating the μ coordinate frame to the λ one ($\mathbf{P}$ is the matrix which transforms λ vectors into corresponding μ ones, expressed in the λ frame, and $\mathbf{p}$, is the relative displacement, expressed in the λ frame, of the μ origin away from the λ origin). In the case of dislocations, Eq. (12) yields $\mathcal{Z}_{\rm ij} = (\mathbf{I}, \mathbf{z}_{ij})$, where $\mathbf{I}$ is the identity rotation, and $\mathbf{b}_{ij} = \mathbf{z}_{ij}$ (other admissible types of defects are discussed by Pond [35]). Interfacial dislocations

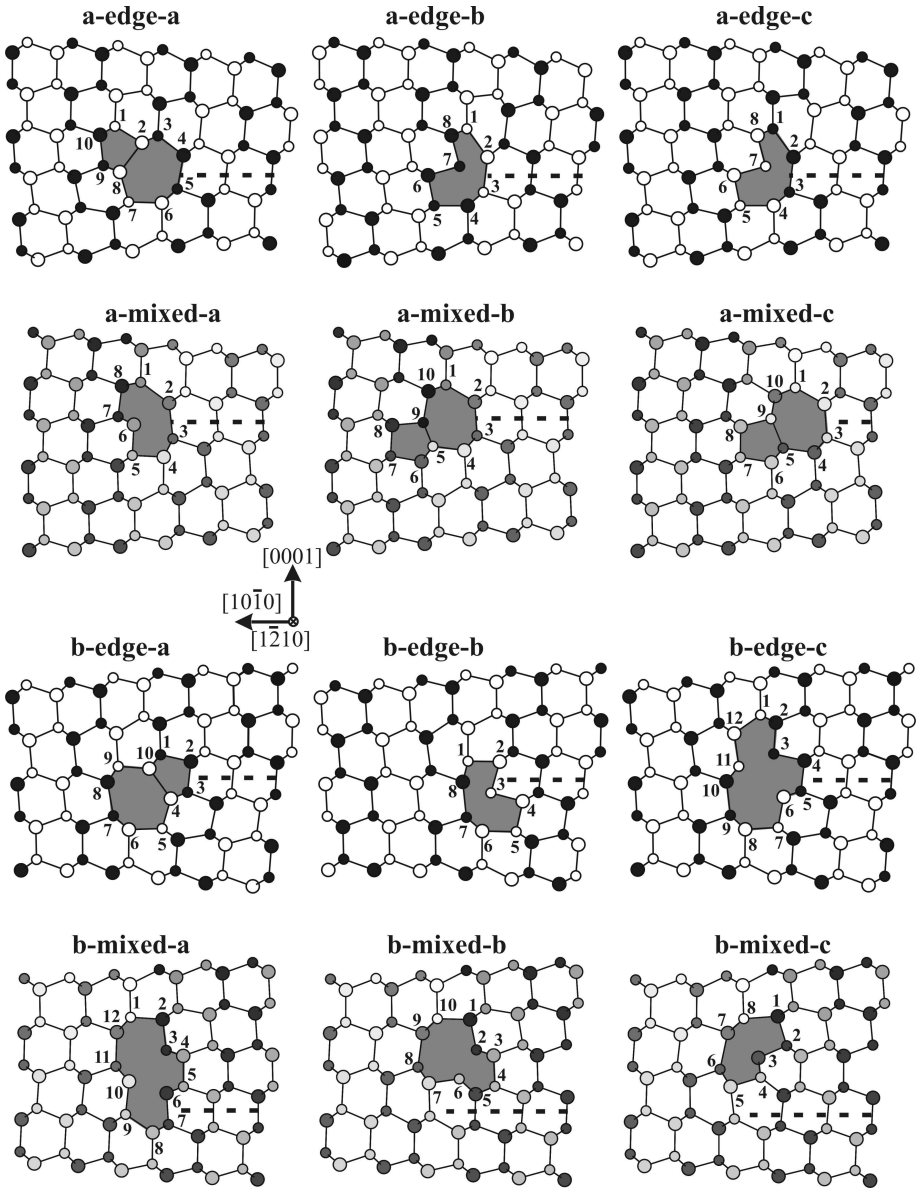

Figure 4: The relaxed atomic core configurations in N-polarity GaN projected along the $[1\bar{2}10]$ direction. Symbols are as in figure 1. Shading of atoms indicates distinct levels along the projection direction. For the edge dislocations there are two such levels i.e. at 0 and $a/2$, whereas for mixed type partials shading denotes multiple different levels. The shaded atomic rings depict the cores of the dislocations. Reprinted figure with permission from [26]. Copyright (2004) by the American Physical Society.

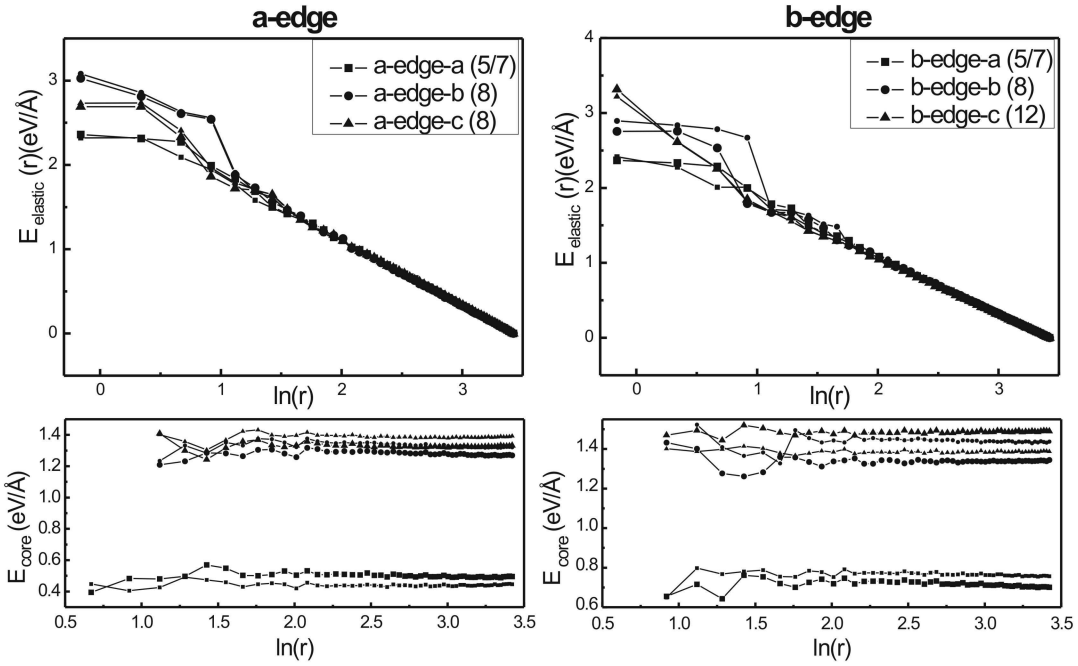

Figure 5: Elastic energy per unit length $\mathrm{E}_{elastic}(r)$ stored in the region bounded by coaxial cylinders of radii r and R_0, and the core energy $\mathrm{E}_{core}(r) = \mathrm{E}_d(r) - \mathrm{E}_{elastic}$ as a function of $\ln(r)$ for the a-edge and b-edge configurations. (Large symbols denote N-polarity whereas small symbols denote Ga-polarity) The core radius r_0 is given by the radius below which linearity breaks down. Reprinted figure with permission from [26]. Copyright (2004) by the American Physical Society.

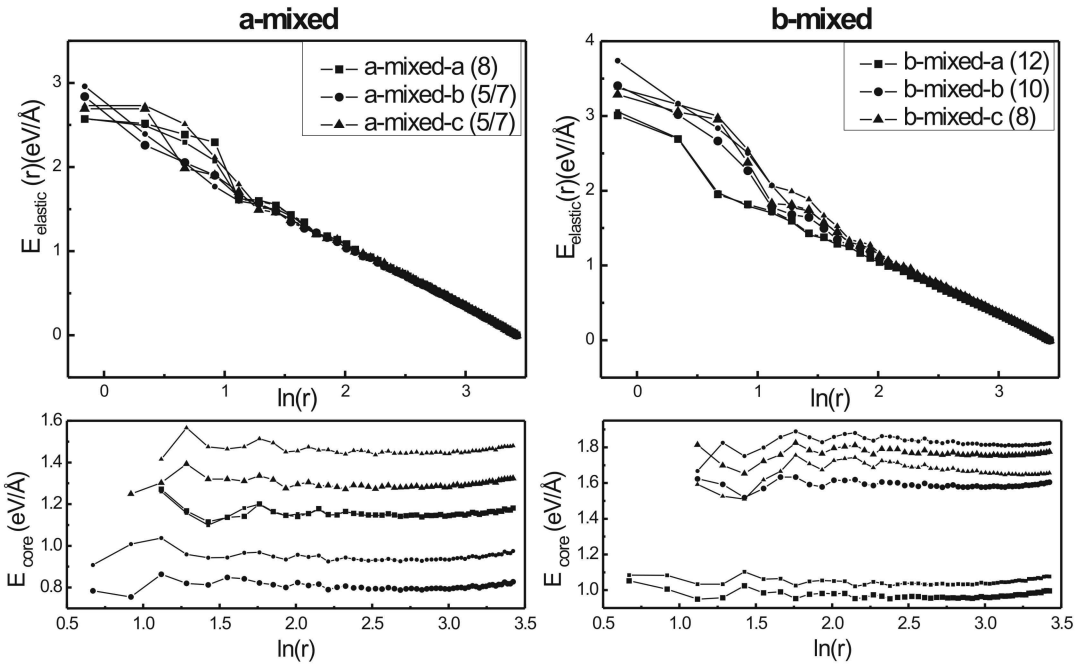

Figure 6: Elastic energy per unit length $\mathrm{E}_{elastic}(r)$ stored in the region bounded by coaxial cylinders of radii r and R_0 and the core energy $\mathrm{E}_{core}(r) = \mathrm{E}_d(r) - \mathrm{E}_{elastic}$ as a function of $\ln(r)$ for the a-mixed and b-mixed configurations. Symbols are as in figure 5. Reprinted figure with permission from [26]. Copyright (2004) by the American Physical Society.

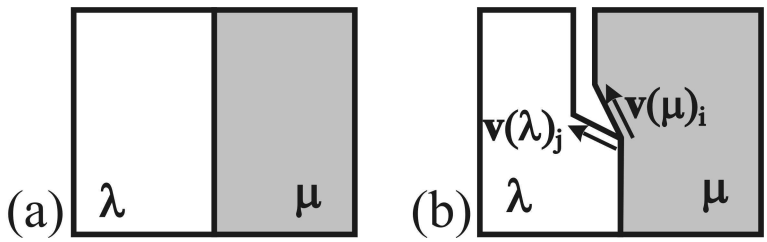

Figure 7: (a) Bicontinuum. (b) Schematic illustration of the introduction of an interfacial dislocation by the Volterra process. Reprinted figure with permission from [25]. Copyright (2001) by the American Physical Society.

can also have associated step character, and this is taken into account by the Volterra approach (figure 7(b)).

In our particular case, we consider the interface to be the $\{10\bar{1}0\}$ IDB and hence $\mathbf{P} = \bar{1}$, the inversion operation, while $\mathbf{p}$ is the relative displacement of the inverse polarity domains. The electronically inert character of one type of inversion domain boundaries (IDBs) has been attributed to a particular relative displacement of the abutting domains leading to the elimination of "wrong" bonds along the IDB plane. Such IDBs have been designated to belong to the IDB* structural model [39] and their observation in GaN specimens has been reported by a number of authors [40] [41] [42]. A second type of IDB, namely the Holt IDB [43], comprises wrong bonds and has been shown to be electrically active [39]. Consequently, it requires a higher formation energy than IDB*s [39]. In figure 8 the atomic structures of the $\{10\bar{1}0\}$ IDB*, and Holt IDB in the GaN wurtzite structure are illustrated. In the $\{10\bar{1}0\}$ Holt-type IDB, $\mathbf{p} = 3/8[0001]$) while, for the IDB*, $\mathbf{p} = -1/8[0001]$. The relative displacement vectors $\mathbf{p}$ are defined taking as reference the Austerman – Gehman IDB model [25] [36] [44].

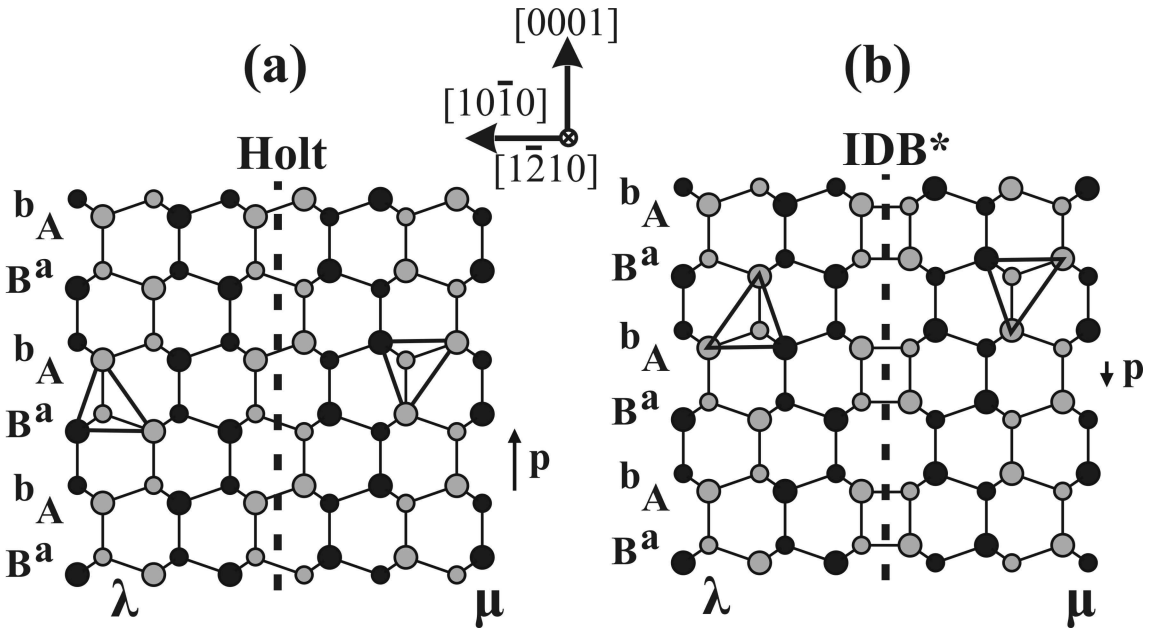

Figure 8: Schematic illustrations of $\{10\bar{1}0\}$ IDBs in the wurtzite GaN structure. (a) Holt-type IDB (p = 3/8[0001]), (b) IDB* (p = −1/8[0001]). ($< 1\bar{2}10 >$ projection, large and small circles denote distinct atomic species, shading indicates levels 0 and $a/2$ along the projection direction, and tetrahedra indicate polarity reversal). The vectors denote displacement of domain μ with respect to domain λ. The stacking sequence along [0001] is also given.

Using the Volterra-like approach, the defect character of IDB junctions with I_1 (0001) SFs can be determined by considering SF-introducing $\mathcal{V}_i$ operations. Two such operations can be distinguished, *i.e.* either $\mathcal{V}_1 = (\mathbf{I}, \mathbf{v}_1)$ where $\mathbf{v}_1 = \pm\ 1/3 < 10\bar{1}0 > + 1/2\ [0001]$, or $\mathcal{V}_2 = (\mathbf{I}, \mathbf{v}_2)$ where $\mathbf{v}_2 = \pm\ 1/6 < \bar{1}010 > + 1/2\ [0001] \pm 1/6 < \bar{1}2\bar{1}0 >$. The signs of the $< 10\bar{1}0 >$ components of $\mathbf{v}_1$and $\mathbf{v}_2$ are reversed when changing the sense of the SF-associated stacking, *i.e.* $\ldots ABABCBCB \ldots$ or $\ldots ABABACAC \ldots$. The corresponding step heights on the $\{10\bar{1}0\}$

plane are $h_1 = \pm\ (3)^{1/2}a/3$ and $h_2 = \pm\ (3)^{1/2}a/6$ respectively.

By employing the aforementioned operations, Volterra-like diagrams of all the admissible junctions of an IDB* with a I_1 SF are illustrated in figures 9(a) to (h), where it can be seen that they lead to transformation of IDB character from IDB* to Holt; the 1/2[0001] component of the SF-introducing operation accommodates the IDB structural transformation. In figures 9(a)-(h) we chose to apply the SF-introducing operation to domain μ while, for domain λ, we may employ either the identity operation (**I**, **0**) or a lattice translation (**I**, $\mathbf{t}(\lambda)$), where $\mathbf{t}(\lambda) = 1/3< 2\bar{1}\bar{1}0 >$. These operations yield the smallest-in-magnitude Burgers vectors for the particular interactions. The Burgers vectors obtained from Equation (12), as well as the average step heights h_{av} on the IDB plane are also given in figure 9.

In addition to applying the SF-introducing operations only to domain μ, we may apply such operations to both the λ and μ domains (figure 9(i) to (l)). These cases correspond to the SF crossing the IDB, and it can be seen that the IDB type remains invariant. In figures 9(i) and (j), the SF crosses via a dislocation-free step whereas, if the SF structural units are mirror related with respect to the IDB plane, a partial dislocation is required (figures 9(k) and (l)).

For the IDB-SF interactions, the supercells corresponding to each Volterra model have been constructed based on figure 9. The energies of the IDBs that appear in the studied interactions, as calculated by the MSWp [19], are E_{HOLT}=166.3 meV/Å^2 and E_{IDB*}=61.4 meV/Å^2.

In the case of IDB-I_1 SF interaction models, due to the existence of three types of planar defects, there is no linear part in the energy versus ln(r) plots. Consequently there is no way to evaluate the core parameters but only the prelogarithmic factors by calculating the slope of the fitted line to the curve. The calculated values of the prelogarithmic factors ($A_e = 0.261\ eV/\mathring{A}$ for the a-model and $A_m = 0.203\ eV/\mathring{A}$ for the f-model) are in satisfactory agreement with the values calculated by elastic theory, ($A_e = 0.258\ eV/\mathring{A}$ for edge type and $A_m = 0.245\ eV/\mathring{A}$ for mixed type using elastic constants calculated by the MSWp [32],) confirming the coherency of the method.

Taking into account the size of our supercells the interaction energy of each interaction model is equal to the core energy plus an elastic contribution. Consequently the interaction energy represents the core energy of each model and due to the fact that all the supercells have the same size, we are able to compare the calculated values between the models with the same Burgers vector.

3.2 Results

Among the twelve models of figure 9, five comprise edge type partial dislocations (**a**, **d**, **e**, **h**, **l**), five involve mixed type dislocations (**b**, **c**, **f**, **g**, **k**), and two models (**i** and **j**) are dislocation-free interactions. Regarding the two dislocation-free interactions, each case can appear in two possible arrangements of the SF structural units before and after the IDB, thus leading to four initial unrelaxed models (**ia**, **ib**, **ja**, **jb**) [25]. Consequently the total number of Volterra models is equal to fourteen. Additionally by taking into account the polarity of the abutting domains, two atomic configurations, one per each polarity, correspond to each of the fourteen models. Hence a total of twenty eight stable atomic configurations of IDB-SF junctions have been calculated.

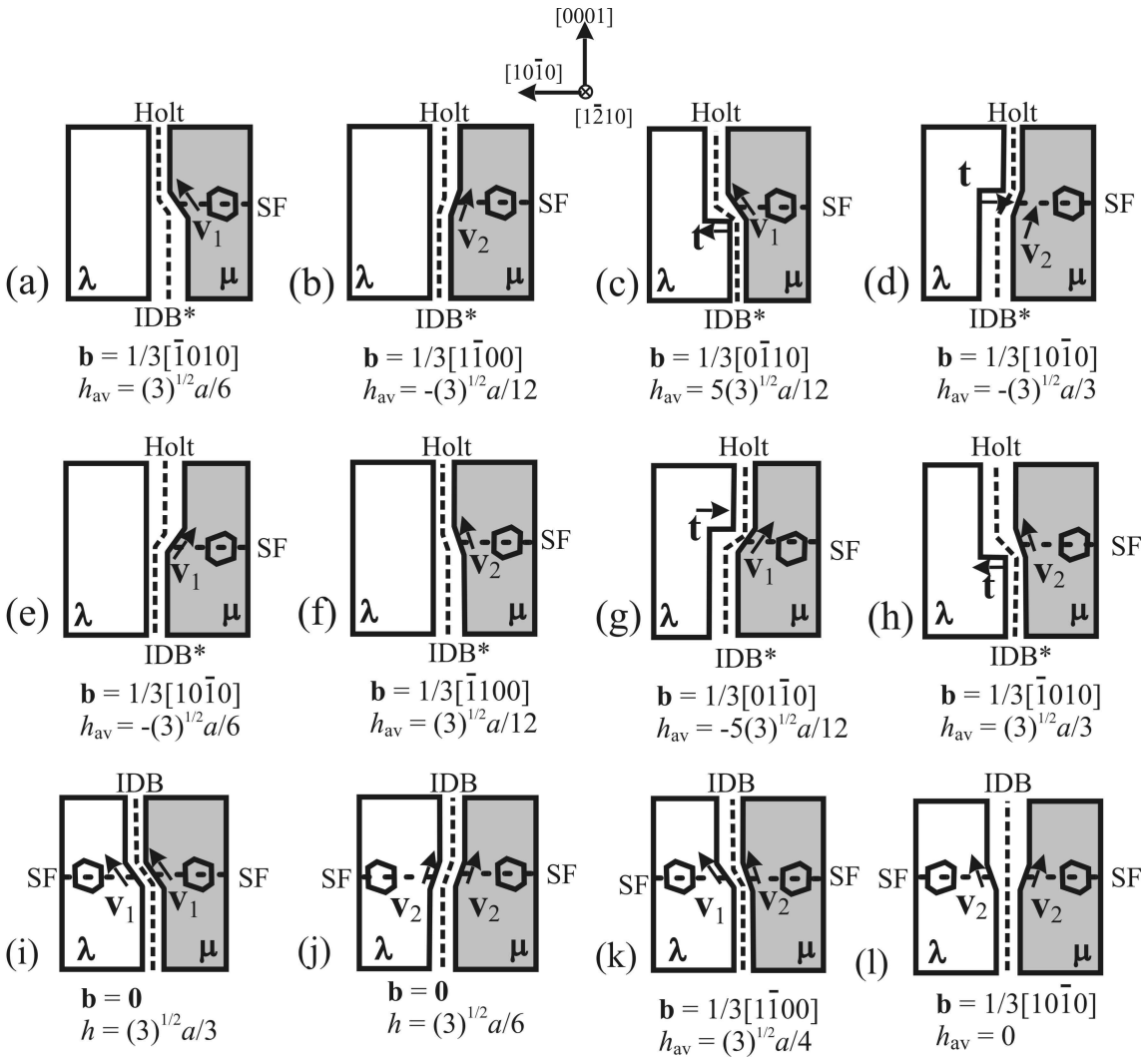

Figure 9: Volterra diagrams of the IDB* - I_1 SF junctions. Junctions (a) to (h) lead to a Holt IDB, while configurations (i) to (l) illustrate IDB - I_1 SF crossings. The IDBs and SFs have been indicated by broken lines. On each SF, a structural unit has been drawn to indicate its sense. The given configurations correspond to minimum Burgers vectors and minimum average step heights (h_{av}). Reprinted figure with permission from [25]. Copyright (2001) by the American Physical Society.

The models **i**, **j**, **k**, and **l**, where the SF crosses the IDB without transforming its character, may be constructed either with IDB* or Holt type IDB. In the present study we examine only crossings involving IDB*s since they are energetically more favourable than Holt IDBs [39].

a) Edge type partial dislocations

The energy calculations indicate that the **a** model has the lowest energy of the edge type models. The relative energies ΔE_{Jn} for the stable atomic configurations of the **a**, **d**, **e**, **h**, and **l** models, taking as reference the lowest energy, are given in figure 10. The associated junction line defects are edge partial dislocations with Burgers vector $b_e = 1/3\,[10\bar{1}0]$.

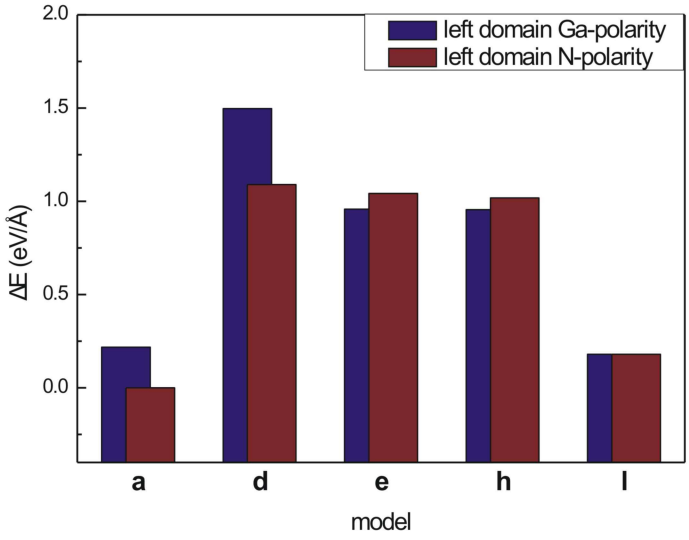

Figure 10: Relative energies calculated by the MSWp, for both polarities of the models a, d, e, h and l. The associated partial dislocations have edge character.

The corresponding relaxed atomic configurations are presented in figure 11.

b) Mixed type partial dislocations

In interactions where the associated junction line defects are partial dislocations with mixed character (i.e. **b**, **c**, **f**, **g**, and **k**) the Burgers vector can be decomposed into a screw $b_{\rm S} = 1/6\,[1\bar{2}10]$ and an edge component $b_{\rm e} = 1/6\,[10\bar{1}0]$. The relative energies as calculated by the MSWp, and taking as reference the lowest energy (**k** model), are given in figure 12.

In figure 13 the relaxed atomic configurations of the models **b**, **c**, **f**, **g** and **k** are presented.

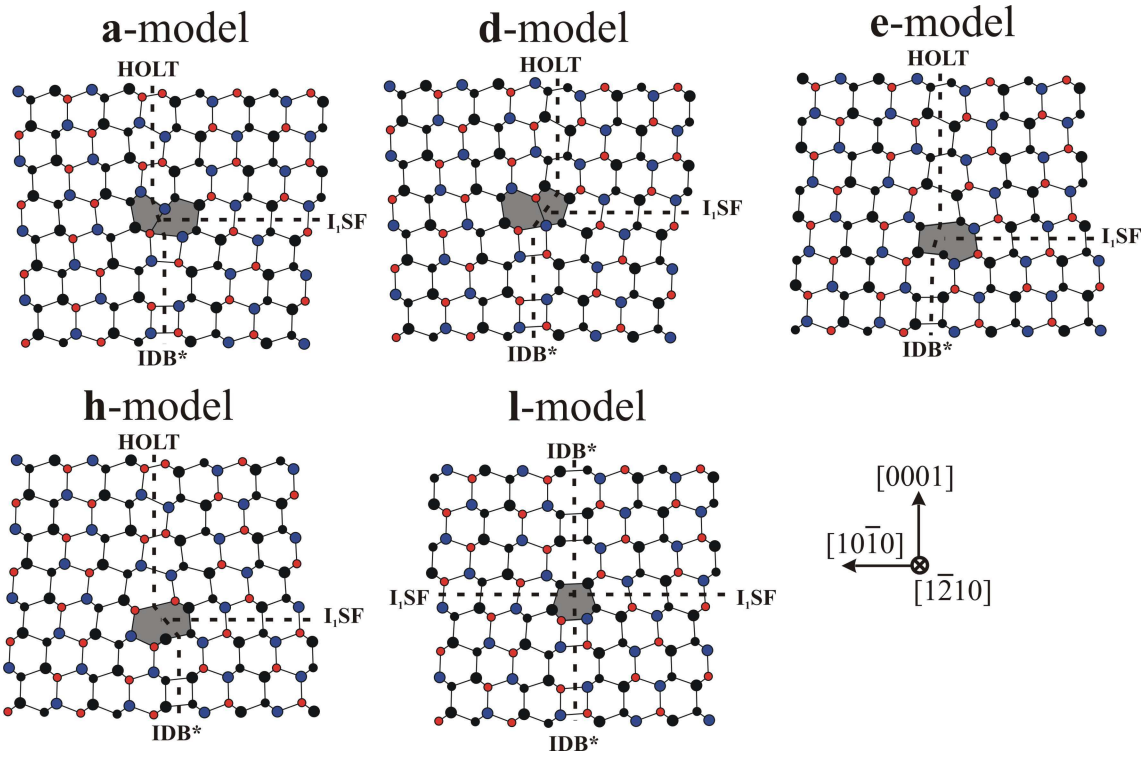

Figure 11: Relaxed atomic configuration of models a, d, e, h and l given in figure 9, which comprise interactions involving partial dislocations with edge character. ($< 1\bar{2}10 >$ projection, broken lines indicate planes of IDBs and SFs, large and small circles denote distinct atomic species, shading of atoms denotes levels 0 and a/2 along the projection direction and the shaded areas represent the central atomic rings of the cores).

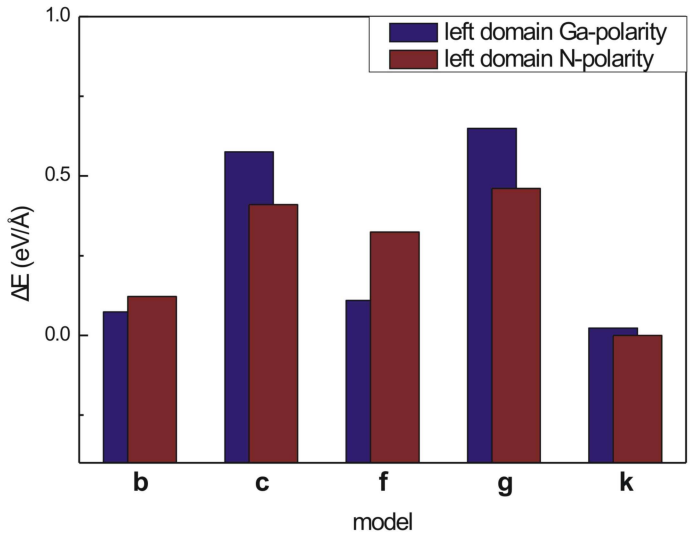

Figure 12: Relative energies of models b, c, f, g, k calculated by the MSWp. The associated junction line defects are mixed type dislocations.

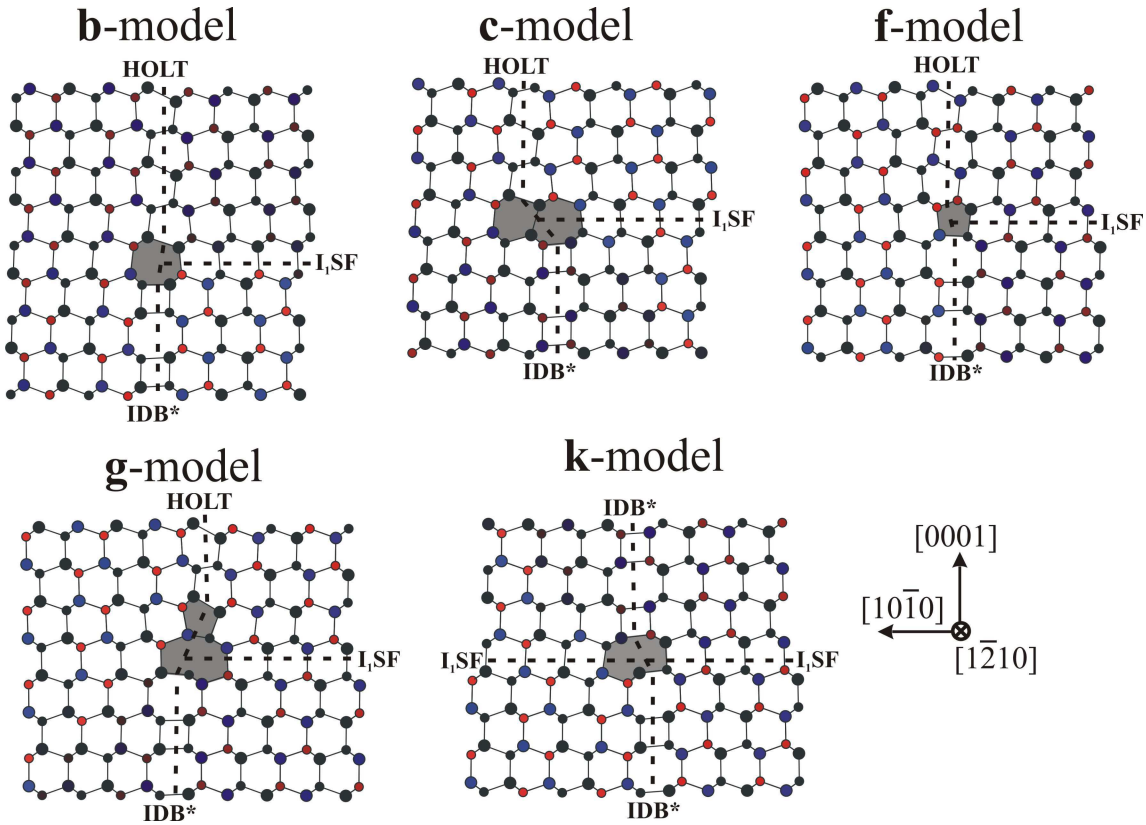

Figure 13: Relaxed atomic configuration of models b, c, f, g and k given in figure 9, which comprise partial dislocations with mixed character. ($< 1\bar{2}10 >$ projection, atoms and symbols are as in figure 11).

c) Dislocation-free interactions.

Two dislocation-free IDB-I_1 SF junctions have been depicted in figure 9 (models **i**, **j**). As it has already been pointed out, each case comprises two possible stable arrangements of the SF structural units before and after the IDB, leading to four models (**ia**, **ib**, **ja**, **jb**) [25]. The relative energy of each configuration, taking as reference the lowest energy, was calculated for both polarities of GaN and the corresponding values are presented in the bar-graph of figure 14.

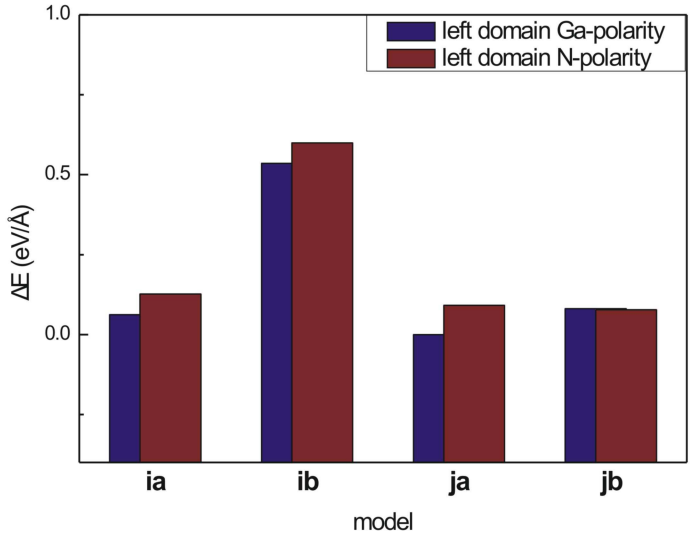

Figure 14: Relative energies of dislocation-free junctions calculated by the MSWp.

In figure 15, the relaxed atomic configurations are presented.

We have presented so far the admissible IDB-SF junctions and a detailed analysis based on the MSWp potential have been presented in ref [27]. It has to be noticed that although the MSWp yields about the maximum accuracy currently possible for the given model sizes, especially for GaN with bulk like coordination of atoms, the energies of the reconstructed cores comprising of Ga-Ga and N-N bond are less accurately represented. However the relaxed models can be used as reference for band structure calculations.

Almost all the relaxed core structures comprise a 5 or 7-atom ring.

Moreover in ref [27], one of the determined core structures has been matched to an IDB-SF junction line observed by high resolution transmission electron microscopy. In particular, this was achieved for the **f**-model which has the second lower energy for the mixed type partial dislocations leading to IDB* transformation to Holt IDB.

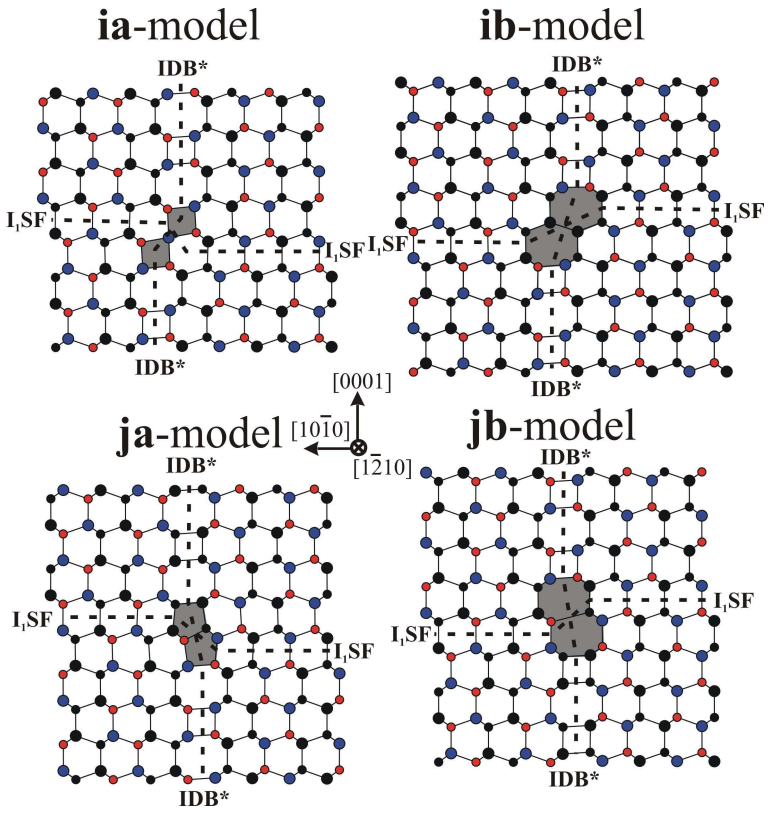

Figure 15: Relaxed atomic configurations of models i and j (figure 9) which comprise dislocation-free interactions. ($< 1\bar{2}10 >$ projection, atoms and symbols are as in figure 11).

4. Conclusions

The atomic structures and dislocations parameters of the $1/6 < 20\bar{2}3 >$ partial dislocations that bound the I_1 SF and the $1/3 < 10\bar{1}0 >$ admissible partial dislocations at the junction lines between I_1 SFs and IDBs have been calculated by means of empirical potential calculations in combination with topological and elastic theory.

Our calculations on $1/6 < 20\bar{2}3 >$ partial dislocations reveal twelve stable configurations in each polarity and their core structures and energies have been presented. Although there are difficulties in determining the exact cylinder radius below which linearity breaks down the core radii have been calculated in the range between 2 and 3.1 Å, and, in all cases, the smallest cores belong to the energetically favourable configurations.

The 5/7 ring core in which the atoms are tetrahedrally coordinated has been found energetically favourable among the edge configurations; such cores have been calculated, in all cases, to have energies less than 0.76 eV/Å. The 8- and 12-atom rings have been found to require energies from 1.28 to 1.48 eV/Å.

Regarding the mixed type partial dislocations, a variety of core configurations (8, 5/7 and 12 atom rings) has been revealed. The 5/7- and 12-atom ring configurations has been found favorable for partial dislocations delineating a I_1 SF formed by a collapsed vacancy disc or a precipitated interstitial loop respectively. However, none of them has been found to consist of only tetrahedrally coordinated atoms. Their core energies are larger than the edge type dislocations and the energetically favourable models were found to require energies from 0.81 to 1.05 eV/Å.

Based on the analysis of ref [26], it is reasonable to postulate that $1/6 < 20\bar{2}3 >$ partial dislocations in wurtzite GaN may introduce band gap states. However, in addition to the core structure, the strain environment in the surrounding crystal plays an important role. Further investigations are required in order to determine their influence on the band structure.

Regarding the IDB-I_1 SF interactions, twenty eight stable configurations of such junctions have been identified, sixteen of them resulting in transformations of IDB* to Holt IDBs. Consequently, the IDB*-I_1 SF interactions appears to be an important mechanism for the introduction of Holt IDBs.

Moreover, the majority of the core structures exhibit either dangling bonds or highly distorted bond angles and lengths [27]. Since gap states may arise from reduced coordination or strained bonds, these dislocations could be electrically active. Furthermore the core stress field could act as a trap for electrically active native defects (e.g. vacancies) or impurities. Consequently almost all the examined junction cores are potentially electrically active defects.

It has also been found that the core energy depends on polarity for dislocations with line direction along $< 1\bar{2}10 >$ [26], [27]. When the polarity of the supercells is inverted, the core ring configuration remains invariant but not the lengths of the bonds and the angles between them. The changes depend on the type of the atoms and the positions of their neighbour atoms.

5. Acknowledgements

This work was supported by PENED 01ED481 project of the GSRT.

References

[1] J. I. Pankove and T. D. Moustakas, in *Semiconductors and Semimetals*, edited by R. K. Willardson and E. R. Weber (Academic Press, New York, 1998), Vol. **50-57**

[2] J. Elsner, R. Jones, P. K. Sitch, V. D. Porezag, M. Elstner, Th. Frauenheim, M. I. Heggie, S. Oberg, and P. R. Briddon, Phys. Rev. Let. **79**, 3672 (1997).

[3] A. F. Wright, and U. Grossner, Appl. Phys. Lett. **73**, 2751 (1998).

[4] K. Leung, A. F. Wright, and E. B. Stechel, Appl. Phys. Lett. **74**, 2495 (1999).

[5] S. M. Lee, M. A. Belkhir, X. Y. Zhu, Y. H. Lee, Y. G. Hwang, and T. Frauenheim, Phys. Rev. B **61**, 16033 (2000).

[6] C. J. Fall, R. Jones, P. R. Briddon, A. T. Blumenau, T. Fauenheim, and M. I. Heggie, Phys. Rev. B **65**, 245304 (2002).

[7] Y. Xin, S. J. Pennycook, N. Browning, P. D. Nellist, S. Sivananthan, F. Omnes, B. Beaumont, J. P. Faurie, and P. Gibart, Appl. Phys. Lett. **72**, 2680 (1998).

[8] Z. Lilienthal-Weber, Y. Chen, S. Ruvimov, and J. Washburn, Phys. Rev. Lett. **79**, 2835 (1997).

[9] P. Venneques, B. Beaumont, M. Vaille, and P. Gibart, Appl. Phys. Lett. **70**, 2434 (1997).

[10] J. W. P. Hsu, M. J. Manfra, S. N. G. Chu, C. H. Chen, L. Pfeiffer, and R. J. Molnar, Appl. Phys. Lett. **78**, 3980 (2001).

[11] J. E. Northrup, Appl. Phys. Lett. **78**, 2288 (2001).

[12] J. E. Northrup, Phys. Rev. B **66**, 045204 (2002).

[13] J. P. Hirth and J. Lothe, *Theory of Dislocation*, **2**nd edition (Wiley, New York, 1982).

[14] F. Stillinger, and T. A. Weber, Phys. Rev. B **31**, 5262 (1985).

[15] J. Kioseoglou, G. P. Dimitrakopulos, H. M. Polatoglou, L. Lymperakis, G. Nouet, and Ph. Komninou, Diam. Relat. Mater. **11**, 905(2002).

[16] J. Kioseoglou, H. M. Polatoglou, L. Lymperakis, G. Nouet, and Ph. Komninou, Comp. Mater. Sci. **27**, 43 (2003).

[17] J. Kioseoglou, Ph. Komninou, G. P. Dimitrakopulos, Th. Kehagias, H. M. Polatoglou, G. Nouet, and Th. Karakostas, Solid State Electron **47**, 553 (2003).

[18] J. Kioseoglou, A. Bιrι, G.P. Dimitrakopulos, A. Serra, G. Nouet, and Ph. Komninou, Phys. Stat. Sol (c) **0**, 2464 (2003).

[19] A. Bιrι, and A. Serra, Phys. Rev. B **65**, 205323 (2002).

[20] A. Bιrι, and A. Serra, Phys. Rev. B **66**, 085330 (2002).

[21] A. T. Blumenau, M. I. Heggie, C. J. Fall, R Jones, and T. Frauenheim, Phys. Rev. B **65**, 205205 (2002).

[22] A. T. Blumenau, C. J. Fall, J. Elsner, R. Jones, M. I. Heggie, and T. Frauenheim, Phys. Stat. Sol. (c) **0**, 1684 (2003).

[23] X. Blase, K. Lin, A. Canning, S. G. Louie, and D. C. Chrzan, Phys. Rev. Lett. **84**, 5780 (2000).

[24] M. Kohyama, Modell. Simul. Mater. Sci. Eng. **10**, R31 (2002).

[25] G. P. Dimitrakopulos, Ph. Komninou, J. Kioseoglou, Th. Kehagias, E. Sarigiannidou, A. Georgakilas, G. Nouet, and Th. Karakostas, Phys. Rev. B. **64**, 245325 (2001).

[26] J. Kioseoglou, G. P. Dimitrakopulos, Ph. Komninou, and Th. Karakostas, Phys. Rev. B. **70**, 035309 (2004).

[27] J. Kioseoglou, G. P. Dimitrakopulos, Ph. Komninou, H. M. Polatoglou, A. Serra, A. Bιrι, G. Nouet, and Th. Karakostas, Phys. Rev. B.(in press)

[28] S. Strite, and H. Morcoc, J. Vac. Sci. Technol. B **10**, 1237 (1992).

[29] G. P. Dimitrakopulos, Ph. Komninou, and R. C. Pond, Phys. Stat. Sol (b) **227**, 45 (2001).

[30] L. Verlet, Phys.Rev. **159**, 98 (1967).

[31] C. Stampfl, and C. G. Van de Walle Phys. Rev. B **57**, R15052 (1998).

[32] N. Aichoune, V. Potin, P. Ruterana, A. Hairie, G. Nouet, and E. Paumier, Comp. Mater. Sci. **17**, 380 (2000).

[33] A. Polian, M. Grimsditch, and J. Grzegory, J. Appl. Phys. **79**, 3343 (1996).

[34] J. Elsner, A. T. Blumenau, T. Frauenheim, R. Jones, and M. I. Heggie, Mat. Res. Soc. Symp. Proc. **595**, W9.3.1 (2000).

[35] R. C. Pond, in *Dislocations in Solids*, edited by F. R. N. Nabarro (North Holand, Amsterdam, 1989), Vol. **8**, p.5.

[36] G. P. Dimitrakopulos, Th. Karakostas, J. G. Antonopoulos, and R. C. Pond, Interface Science **5**, 35 (1997).

[37] V. Volterra, Ann. Sci. Ec. Norm. Sup. Paris **24**, 401 (1907).

[38] T. Hahn, in *International Tables for Crystallography*, edited by T. Hahn (Reidel, Dordrecht, 1983).

[39] J. E. Northrup, J. Neugebauer, and L. T. Romano, Phys. Rev. Lett. **77**, 103 (1996).

[40] J. L. Rouviere, M. Arlery, B. Daudin, G. Feuillet, and O. Briot, Mat. Sci. Eng. B **50**, 61 (1997).

[41] V. Potin, G. Nouet, and P. Ruterana, Phil. Mag. A **79**, 2899 (1999).

[42] Ph. Komninou, Th. Kehagias, J. Kioseoglou, E. Sarigiannidou, Th. Karakostas, G. Nouet, P. Ruterana, K. Amimer, S. Mikroulis, and A. Georgakilas, Mat. Res. Soc. Symp. Proc. **639**, G3.47 (2001).

[43] D. B. Holt, J. Phys. Chem. Solids. **30**, 1297 (1969).

[44] S. B. Austerman and W. G. Gehman, J. Mater. Sci. **1**, 249 (1966).